Ind. J. Pharm. Edu. Res., 2024; 58(3s):s787-s795.
https://www.ijper.org

Original Article

Interstitial Lung Diseases Classification in the Context of Pharmaceutical Education and Research: A Two-Level Deep Learning Approach

Vanita Dnyandev Jadhav[1,*], Lalit Vasantrao Patil[2]

[1]Department of Computer Engineering, SKN College of Engineering, Vadgaon, Pune, Maharashtra, INDIA.
[2]Department of Information Technology, SKN College of Engineering, Vadgaon, Pune, Maharashtra, INDIA.

ABSTRACT

Aim/Background: In this work, a novel method for improving the quality of healthcare in the diagnosis of Interstitial Lung Disease (ILD) using High-Resolution Computed Tomography (HRCT) images is proposed. **Materials and Methods:** In contrast to previous research that necessitated the human identification of Regions of Interest (ROI), a two-phase deep learning method is presented. First, multi-scale feature extraction is used to precisely segment the lung in HRCT images using a conditional Generative Adversarial Network (c-GAN). A Support Vector Machine (SVM) classifier classifies the characteristics extracted by a pretrained ResNet50 from the segmented lung image into seven ILD classes in the second step. **Results:** The two-step approach that is being offered improves efficiency by doing away with the necessity for ROI extraction. The superiority of the method is demonstrated by performance comparison with patch-based and whole-image-based algorithms. The suggested method reduces false alarms by achieving a maximum classification accuracy of 94.65% for the normal class. Despite having the lowest accuracy (84.12%), the consolidation class performs better than other whole-image-based methods. **Conclusion:** The suggested two-stages ILD classifier performs much better due to the step-by-step improvement in the deep learning method. This work lays the groundwork for advanced decision support systems in the pharmaceutical industry and advances pharmaceutical research and education. The method proposed improves knowledge of the pathophysiology of ILD and allows for customized treatment approaches.

Keywords: Deep learning, Interstitial lung disease, Support vector machine, Lung segmentation, Lung Classification.

Correspondence:
Mrs. Vanita Dnyandev Jadhav
Department of Computer Engineering, SKN College of Engineering, Vadgaon, Pune, Maharashtra, INDIA.
Email: vanjadhav19@gmail.com

Received: 14-11-2023;
Revised: 23-02-2024;
Accepted: 01-06-2024.

INTRODUCTION

Finding the precise kind of ILD is crucial to creating effective treatment plans since Interstitial Lung Disease (ILD) patients have a significant risk of developing lung cancer. Precisely and promptly identifying the many forms of ILDs is essential for customizing targeted treatment plans, which is why pharmaceutical education and research have a strong interest in this crucial field. Data-driven decision-making is growing in popularity in the healthcare sector as a result of its speedy collection and accurate analysis of entire data.[1] It forces the decision-makers to pick the best course of action, make predictions about the future and create long-term plans. Diagnose a certain ILD type, predict ILD spread and subsequently execute preventive measures are all related to ILD categorization issues. The initial screening method for rapid imagining of regular and irregular cases of any illness is HRCT image-based processes. Additionally, the data-driven method of categorizing ILD can be active in noticing ILD at an initial stage.

Goal of the current study is to enhance ILD classification performance by investigating a multistep deep learning network. By encouraging the creation of cutting-edge diagnostic tools, this strategy not only aims to increase the precision of ILD categorization but also makes a positive impact on the rapidly developing fields of pharmaceutical education and research. This research aims to promote pharmaceutical research and teaching in the field of respiratory disorders by providing a comprehensive framework and shedding light on the possibilities of sophisticated computational tools in altering ILD diagnoses.

Below are the key points of suggested method for classifying ILDs:

The suggested approach makes use of entire HRCT images to do away with the need for physical ROI extraction of ILD-infested lung tissue.

DOI: 10.5530/ijper.58.3s.80

In the suggested method, the first step involved precise lung segmentation utilizing a c-GAN with a MSFE module from HRCT images with lung anomalies. By removing the undesirable background from HRCT pictures, lung segmentation enables the subsequent deep learning procedure to concentrate on ILD features of lung.

In second step, the segmented lung pictures were used to abstract the profound features using ResNet50. Additionally, segmented lung pictures from various ILD classes were used to fine-tune the pretrained ResNet50 by means of the transfer learning methodology.

Lastly, SVM classified the 10 ILD classes- bronchiectasis, normal, ground glass, cysts, fibrosis, tuberculosis, emphysema, consolidation, micronodules and macronodules -using deep features from ResNet50.

The projected algorithm's performance is compared to that of existing patch-based and whole picture input approaches.

Literature Survey

In the image-based classification method, the ILD class is labelled and features are mined so as to train the classifier. For longitudinal and frequency-based picture examination, feature extraction comprises effective form, texture and color extraction. Gray level values,[2] statistic filters like run length and grey level co-occurrence matrix, texture feature extraction,[3] spatial and shape features[5] and edge features like Gaussian and Wavelet filters[4] are a few of these techniques. These attributes won't, however, be able to capture the deep learning aspects that deep learning algorithms have suggested. The reliability of feature extraction to analyze medical images has increased with development of deep learning algorithms. These methods are employed in the detection, segmentation and classification fields to address a variety of applications.[6-8] To create deep feature vectors, deep learning procedures like AlexNet, GoogLeNet and VGG are used.[9-11] The huge volume of data required for testing and training in this architecture, however, makes it challenging in the medical industry and occasionally tiresome and slow. This problem of data shortage, can outcome in overfitting, which is addressed by transfer learning,[12] conserves the information gained from a data-rich cause domain. Following the proper feature extraction, these features are labelled in order to apply the machine learning procedures. K-nearest neighbours, Support vector machines, Bayesian classifiers, artificial neural networks and linear discriminant analysis are the best widely used supervised classification techniques.[13-15] SVM is the classifier that offers the best value in terms of actually positive rates and correctness. Santosh *et al*. have provided a thorough analysis of deep learning methods for resolving numerous medicinal imaging issues.[16] The majority of ILD classification studies are based on picture representation using ROI patching. Li *et al*. considered a narrow convolution coating to automatically and successfully categorize ILD and study significant image features from lung image areas.[17] For the categorization of ILDs, Anthimopoulos *et al*. devised and evaluated a CNN with a leaky ReLU activation function.[18] An approximate 85.5% classification performance is shown by the ILD of seven patterns. Doddavarapu *et al*. developed a framework for CNN for automatic ILD classification.[19] To enhance ILD classification performance and demonstrate a considerable performance gain over former CNNs ResNet, VGGNet and, AlexNet, Guo *et al*. designed a better DenseNet termed small kernel DenseNet.[20] Poap and Sahlol *et al*. demonstrated an alternative method based on entire X-ray pictures to identify lung illnesses and diagnose Tuberculosis (TB).[21,22] In order to support automatic lung nodule segmentation and classification with increased accuracy, Khan *et al*. have suggested a system that uses VGG-SegNet to extract nodule and pretrained Deep Learning-created organization to make it easier to identify lung nodules automatically.[23]

The literature review reveals the following crucial gaps that can be filled using the suggested strategy:

Utilizing the ROI patch, which is labor-intensive and needs professional assistance,

The pictorial particulars and geographical context may not be adequately captured by the small HRCT patches,

The segmentation of lung nodules using conventional image processing algorithms and

The majority of classifiers established in literature employ directly ROI patches, in its place of creating the classifier directly from HRCT images.

Architecture of Proposed Method of Deep Learning Networks

The majority of ILD classifiers now in use need manually identifying Regions of Interest (ROI) in order to monitor for possible illness. To map the ILD classes, deep learning algorithms have also been fed the ROI patches. The 2-step construction of a deep learning procedure, which associates two distinct deep learning procedures used for extraction of deep features and classification of ILD, has been proposed in this paper. The two-step deep learning network technique for ILD classification is shown in Figure 1. This strategy takes the entire collection of HRCT imageries as input and outputs the classification of ILD. By reducing background noise, the initial step of the deep learning system separates the lung portion from the provided HRCT pictures. As a result, the second step's feature extraction process used another deep learning algorithm to extract the features from segmented lung HRCT from first step. Additionally, the second step deep learning technique used Support Vector Machine (SVM) which is memory-efficient classifier, to categorize ILDs founded on the features gathered.

Step 1: Lung Segmentation using C-GAN

Because it has generator (G) and discriminator (D) as its two primary subcomponents, C-GAN is ideal to utilize for segmentation purposes.[24] The generator's job is to produce false images from latent samples. Additionally, the generator is trained to translate these arbitrary variables into identifiable visuals, deceiving the Discriminator (D). The Discriminator (D) makes a distinction among the output of generator and reference lung segmentation map, While Generator (G) transfers reference lung segmentation map to the input lung HRCT portion as G: {x, z} y. Suggested C-GAN architecture, depicted in Figure 2, is made up of encoder and decoder slabs and a Multi Scale Feature Extraction unit.

The encoder/decoder blocks were built using ReLU nonlinear action function and size 3 x 3 convolution/deconvolution filters. These blocks create additional normalised instance-normalized feature maps by encrypting the input lung HRCT slices.[25] So as to increase the receptive fields, the feature maps are further down sampled in encoder blocks. In order to preserve the network's symmetry, these characteristics were up sampled by a factor of 2 in the decoder blocks.

The purpose of multi-scale feature extraction is to extract features from lung HRCT scans that address dense abnormalities of various sizes, textures and shapes. The majority of current lung segmentation procedures do not take into account these dense anomalies, which are particularly prevalent at the lung boundary. The suggested approach captures the feature owing to change in

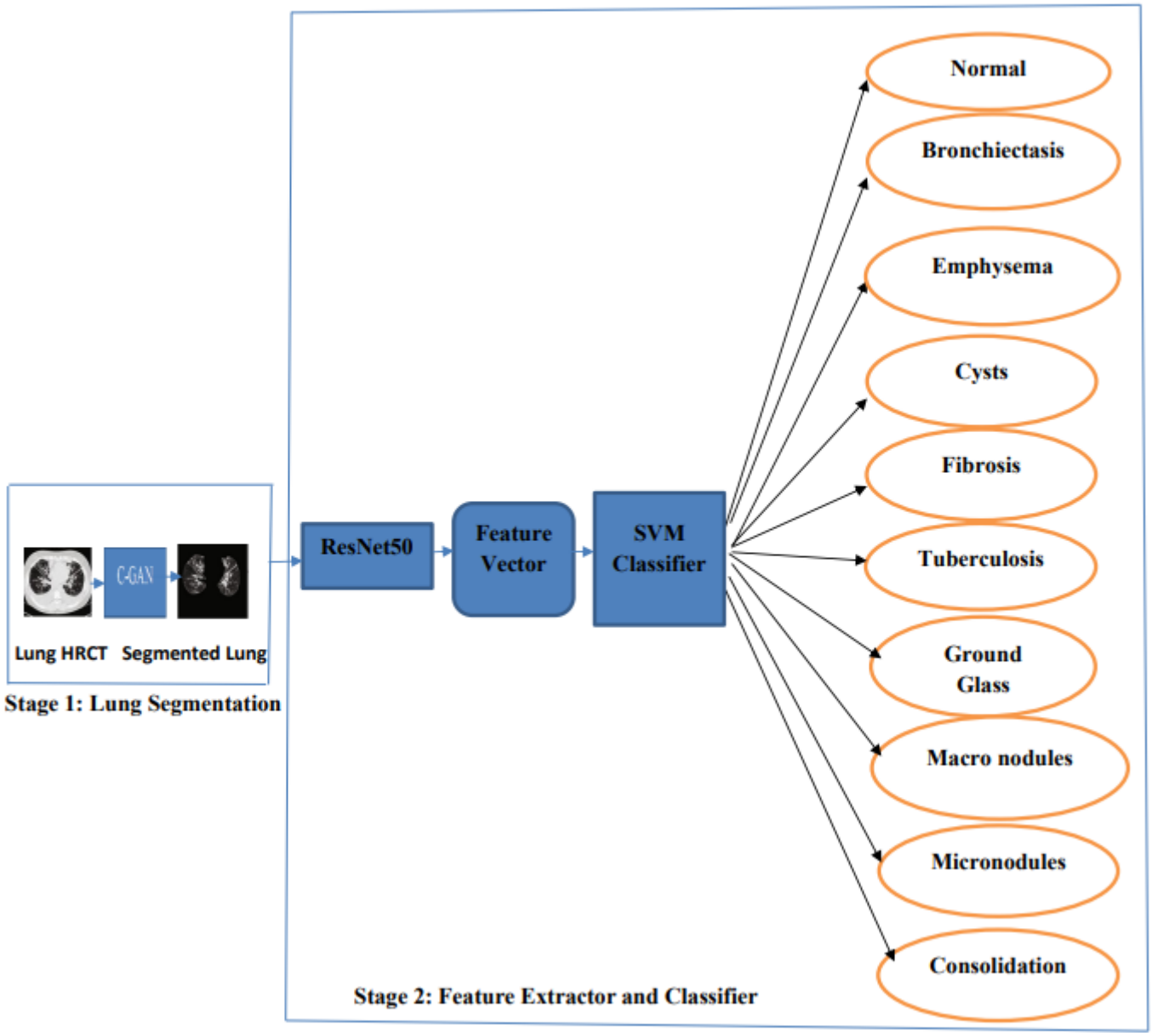

Figure 1: Two-step deep learning network strategy for ILD classification.

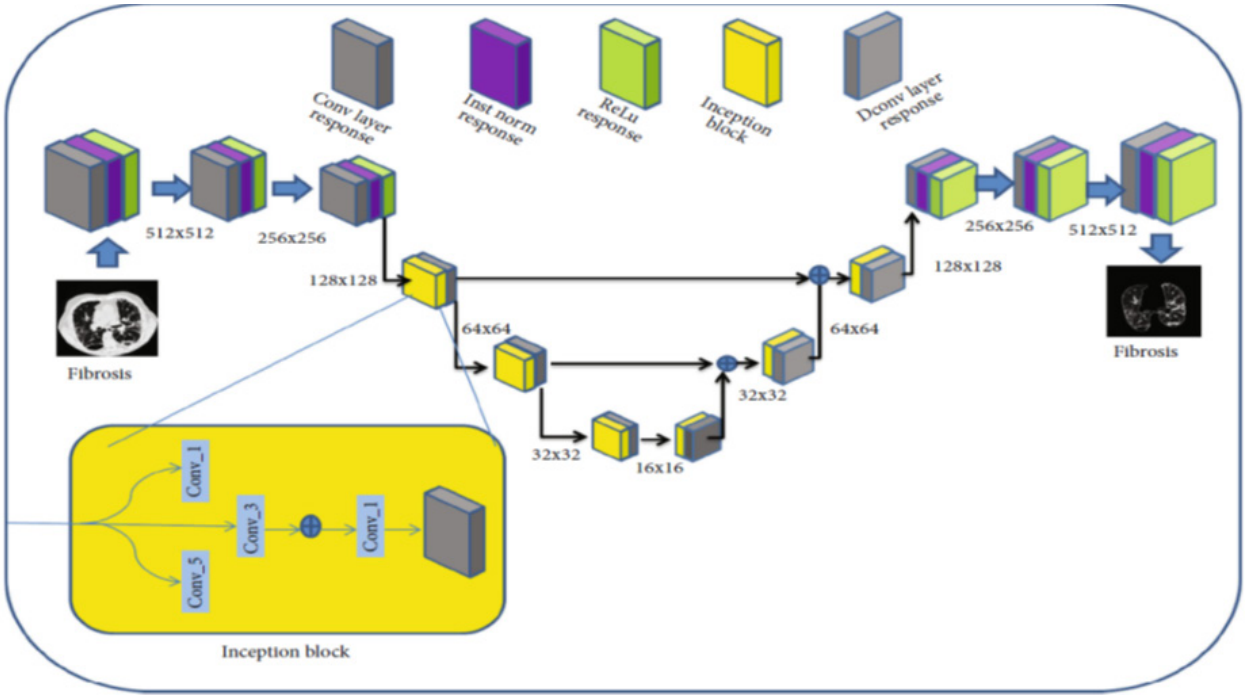

Figure 2: C-GAN Architecture of Lung Segmentation (Step 1).

the presence of anomalies by incorporating multi-scale feature extraction. The MSFE has initialization blocks that consist of 3 convolution layers of filter size-namely, 1x1, 3x3 and 5x5-before the ReLU and instance normalization. Six MSFE modules make up the projected c-GAN segmentation architecture, as depicted in Figure 2. The multiscale features are processed by the first three MSFE modules using a straightforward convolution layer. The processing of these characteristics over a basic deconvolution layer with an up-sampling factor of 2 is how the next 3 MSFE modules preserve symmetry.

During the anticipated c-GAN network's training, the generator and discriminator losses were calculated. The overall loss for the real and fake photos is known as the discriminator loss. The variables of the discriminator and generator have been updated independently. Objective function has been solved in order to train the projected c-GAN network by Adam's optimization method:

$$G^{*}= \arg {}_{G}\min_{D} \max \ell (G,D) \quad (1)$$

The total loss function is specified by,

$$\ell(G,D)=\ell cGAN(G,D) + \lambda \ell L1 (G). \quad (2)$$

The multi-objective probabilistic function of C-GAN ℓcGAN(G,D) and the traditional loss ℓL1 (G) can be stated as,

$$\ell cGAN(G,D)=Ex,y[\log D(x,y)]+Ex,z[\log(1-D(x,G(x,z)))],$$

$$\ell L1 (G) =\sum_{i,j}\|G(x,z)_{i,j} - y_{i,j}\|_{2} \quad (3)$$

Goal of the training is to make discriminator more likely to use training data and less likely to use data tested from the generator. Additionally, the generator has been trained to focus the reverse goals while simultaneously exploiting the likelihood that the discriminator is assigning to its samples.

Step 2: Feature Extraction using ResNet50 and Classification using SVM

Figure 1 shows the result of ResNet50's deep feature extraction on the segmented lung picture from step 1. A multilayer CNN called ResNet50 is constructed on feature spread to avoid gradient vanishing, allowing for the efficient training of considerably deeper networks than those previously employed.[26] ResNet50 is a 177-layer, 50-layer residual network architecture that is built on the idea that a deeper network performs better than a narrow network. A section of the ImageNet database, which can be accessible at http://www.imagenet.org, has been pretrained on by the ResNet50. Table 1 displays the architecture details.

The ResNet50 network is made up of all the same deep network elements like pooling, convolution, fully linked layers and activation piled on top of one another. The self-connection between the layers is the single characteristic that distinguishes it as a residual network. The vanishing gradient issue is solved through identity connections. Gradients will eventually reach the early layers after the residual blocks have been immediately skipped, which will assist in learning the proper weights. The ReLU function, which is used in ResNet50, comes after the addition operation. Four layers and 224x224x3 input images are supported by the ResNet50 architecture, which is depicted in

Table 1: Information about the ResNet50 for step 2's deep features extraction.

Layer Name	Optimal Size	Sub Layer
CONV1	112 X 112	7 X 7, 64, stride 2 3 X 3 max pool stride 2
CONV2_x	56 X56	1 X 1, 64 3 X 3, 64 X 3 1 X 1, 128
CONV3_x	28 X 28	1 X 1, 128 3 X 3, 128 X 4 1 X 1, 512
CONV4_x	14 X 14	1 X 1, 256 3 X 3, 256 X 6 1 X 1, 1024
CONV5_x	7 X 7	1 X 1, 512 3 X 3, 512 X 3 1 X 1, 2048
FLOPs	1 X 1	Average pool, 1000-d fc, softmax 3.8 X 10^9

Table 1. The network uses kernel sizes of 7 by 7 and 3 by 3 for the initial convolution and maximum pooling, respectively.

In addition, level 1 has 3 residual blocks, each with 3 layers and convolution procedures applied to each layer. These 3 layers, which together make up the bottleneck design, are 1x1, 3x3 and 1x1 convolutions. As a result, the three blocks of level 1 have three identity connections. The convolution operation between levels 1 and 2 has been carried out using second step, which doubles the channel width. Similar to this, for the following two levels, as one level is followed by another, the input sizes are halved in height and width and the channel width is doubled.

The SVM is given deep features acquired from a specific layer of ResNet50 for ILD classification. In each layer, network captures a variety of deep features related to classification before moving on to the subsequent layer. The activation's minibatch size of 64 allows the picture dataset to fit in the GPU's memory. Fitting has been done using the activation function's output during SVM training.

EXPERIMENTAL RESULTS

Database, ILD produced by Depeursinge *et al.*[27] was used to analyse the predicted ILD classifier's performance. The chosen ILD database, which contains 108 HRCT images with marked lung field maps, offers a common testing ground for automated ILD analysis algorithms. For the purposes of the analysis, the ten classes of pictures that were taken into consideration in the study were normal, bronchiectasis, emphysema, cysts, fibrosis, tuberculosis, consolidation, macronodules, micronodules and ground glass. The training dataset was created by selecting ILD dataset from 108 HRCT images and projected optimal lung segmentation network was validated using the remaining dataset. The data augmentation strategy, which takes into account the flip right, flip left, flip up, flip down and picture transpose operators to expand the training dataset size, resulted in around 6500 HRCT slices, which were used to train the network.

Cancer Treatment

When drugs are administered in combination regimens or in conjunction with thoracic radiation, which is separately linked to lung fibrosis, it might be difficult to pinpoint the precise causal agents in oncology. Bleomycin, gemcitabine, immune checkpoint inhibitors, EGFR-directed therapy, Mechanistic Target of Rapamycin protein (MTOR) inhibitors and Epidermal Growth Factor Receptor (EGFR)-directed therapies were found to be the most often occurring individual cancer medications that cause Drug-Induced Interstitial Lung Disease (DIILD). It was also discovered that methotrexate is utilised to treat rheumatological disorders and cancer.

Bleomycin damages the lungs through immune-mediated and direct toxic effects. It is mostly used to treat Hodgkin's lymphoma and germ cell tumours. A death rate of up to 48% is related with the indicated risk of 6.8-21%. Bleomycin lung damage might appear asymptomatically; however, its clinical manifestation is quite varied. Imaging is used alone to detect up to 39% of cases. Changes in pulmonary physiology are frequent and include a reduction in the lung's early capacity to Diffuse Carbon Monoxide (DlCO), which is followed by modifications in Forced Vital Capacity (FVC), which is correlated with a decline in symptoms.[30-34]

DIILD can happen at any point while receiving treatment. A study involving patients with germ cell tumours receiving high-dose bleomycin revealed a median of 4.2 months between the start of bleomycin and DIILD. Recent developments in the absence of bleomycin in certain patients with Hodgkin's lymphoma guided by positron emission tomography have been linked to a notable decrease in pulmonary toxicity.

Breast cancer, pancreatic cancer and Non-Small Cell Lung Cancer (NSCLC) are among the malignancies that can be treated with gemcitabine. With documented incidence rates of 1-20%, the risk of DIILD is highest when used in conjunction with other medications, particularly bleomycin, erlotinib and taxanes. The death rate is typically modest, with the exception of severe instances that necessitate hospitalisation, where the rate might exceed 20%. Compared to bleomycin, there is less consistency in the dose-relationship and onset timing.

Table 2: A comparison of the average J and DSC for lung segmentation using c-GAN and present techniques.

Disease	Performance	Proposed Study	UNet	NMF	VGG16	ResNet	MobileNet
Fibrosis	DSC	0.9567	0.9485	0.7681	0.9295	0.9126	0.9040
	J	0.9291	0.9117	0.6600	0.8742	0.8681	0.8330
Consolidation	DSC	0.9713	0.9500	0.8775	0.9479	0.9440	0.9436
	J	0.9467	0.9148	0.7963	0.9031	0.9076	0.8954
Emphysema	DSC	0.9379	0.9629	0.9214	0.9452	0.9261	0.9380
	J	0.9205	0.9340	0.8917	0.8963	0.8975	0.8841
Ground Glass	DSC	0.9559	0.9534	0.8335	0.9444	0.9351	0.9291
	J	0.9283	0.9191	0.7473	0.8975	0.8987	0.8706
Micro nodule	DSC	0.9813	0.9807	0.9678	0.9751	0.9674	0.9586
	J	0.9645	0.9627	0.9391	0.9523	0.9379	0.9210
bronchiectasis	DSC	0.9435	0.9423	0.9207	0.9323	0.9214	0.9134
	J	0.9345	0.9305	0.9111	0.9212	0.9123	0.9054

Agents Targeted at the Epidermal Growth Factor Receptor (EGFR) Small molecule Receptor Tyrosine Kinase Inhibitors (RTKIs) and monoclonal antibodies licenced for the treatment of colorectal, breast and NSCLC are examples of EGFR-targeted medications. With a linked mortality rate of 22.8%, the reported incidence of DIILD for the EGFR-RTKIs gefitinib and erlotinib is 1.2-1.6%. With studies of gefitinib and erlotinib indicating the highest prevalence within 4 weeks of initiating treatment, DIILD with EGFR-RTKIs appears to be an early occurrence.

Mechanistic Target of Rapamycin Protein (MTOR) Inhibitors

MTOR inhibitors are primarily utilised as anti-rejection drugs in solid organ transplantation, as well as in the treatment of neuroendocrine tumours and renal cell carcinomas. There has been evidence linking sirolimus, temsirolimus and everolimus to pulmonary toxicity. A meta-analysis encompassing 2233 cancer patients treated with everolimus across five clinical trials revealed an incidence of DIILD of 2.4% for grades 3-4 and 10.4% for all grades.

Computerised Tomography (CT) data from temsirolimus and everolimus clinical trials were subjected to post hoc analysis, which revealed a considerably greater prevalence of radiographic abnormalities associated with DIILD.

Performance of Lung Segmentation

The Jaccard index (J) and Dice Similarity Coefficient (DSC) are used to represent the c-GAN network's lung segmentation performance.

$$DSC= (2|G(x)\cap y|)/(|G(x)| + |y|)$$

$$J=DSC/(2-DSC) \quad (4)$$

Where G(x) is Generators output and y is reference lung segmentation map.

Due to the dark anomalies found in lung HRCT pictures of various sizes, textures and shapes that are present in the presence of ILD, the lung segmentation performance typically degrades. The typical lung segmentation routine assessment of the c-GAN to other cutting-edge deep networks, such as NMF,[28] UNet,[29] and ResNet,[26] is compared in Table 2, on 42 lung CT images from the ILD collection. The c-GAN technique utilized herein study performs better than other lung segmentation techniques already in use. Figure 3 shows sample images of lung segmentation of fibrosis pattern.

Performance of ILD Classification

In the second step, deep features were mined using pre-trained ResNet50 plotting to the ILD classes using segmented pictures categorized with seven ILD classes: consolidation, normal, fibrosis, emphysema, bronchiectasis, micro nodule and ground glass. Figure 4 displays sample HRCT segmented and original images for each of the seven ILD classifications. By augmenting the database with more images, the over fitting in image recognition training has been reduced.

The pre-trained ResNet50 was given these images in order to extract the deep features. At this point, selecting the right feature layer is crucial for enhancing the classifier's performance.

The weights of previous layers in the pre-trained network that were left alone during the fine-tuning phase are frozen. As a result, transfer learning methods used for ResNet50 are useful for resolving such difficulties since they get around the problem of not having enough radiological pictures to improve the performance of deep learning. With less training data and more efficiency, the transfer learning method creates classification algorithms for medical image data.

Recall, Accuracy, F-score and Precision are performance metrics used to assess classification performance.

$$\text{Recall}=TP/(TP+FN),$$

$$\text{Precision}=TP/(TP+FP),$$

$$\text{F-score}=2TP/(2TP+FP+FN),$$

$$\text{Accuracy}=(TP+TN)/(TP+TN+FP+FN) \quad (5)$$

Where TP is true positives, FP is false positives, TN is true negatives and FN is false negatives.

Table 3 shows ILD Classifier collaborative performance of the projected algorithm.

Table 4 compares the performance of the proposed classifier with the earlier works in the literature. Thus, the proposed classifier performs better even with seven ILD classes. The automatic pretreatment of undesirable noisy regions of HRCT images by the stage 1 lung segmentation procedure increases the projected algorithm's accuracy.

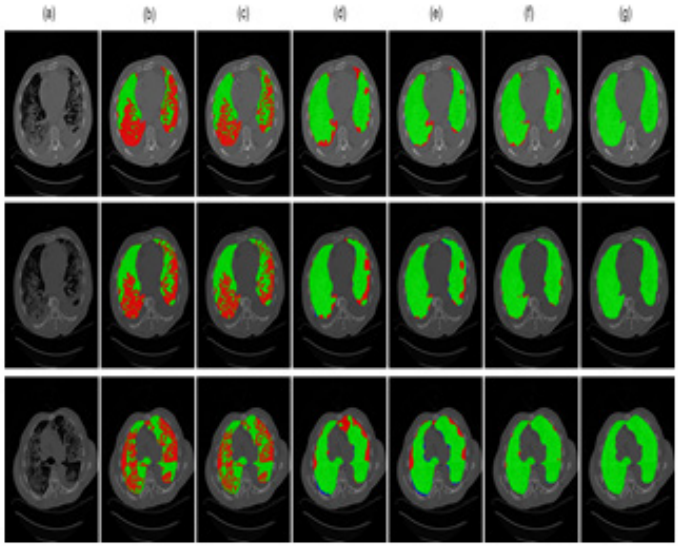

Figure 3: Sample images of lung segmentation of fibrosis pattern. (a) Input lung CT slice (b) VGG16 (c) NMF (d) U-Net (e) ResNet (f) Proposed Network (g) Ground truth.

ILD Classification Process Implementation

The two-step mix deep learning network strategy for ILD cataloging was trained on a computer with an Intel Core i7 processor running at 4.20GHz and an NVIDIA GTX 1080 8GB GPU. The c-GAN network, a shallow network, took roughly 2000 sec to complete segmentation training consuming about 4000 imageries. On other side, training SVM took about 17.85 sec and 19.20 sec were needed to train ResNet50 for profound feature extraction using about 1000 imageries. The overall time needed for each image through testing of the two-step mix technique was approximately 0.7 sec, which is made up of approximately 0.5 sec for step 1 and approximately 0.2 sec for step 2. As a result, the time prerequisite study shows that the ILD classifier's two-step mix technique did not require much additional processing time despite providing the benefit of increased cataloging accuracy.

DISCUSSION

The stated ILD classification method relies on making use of the entire HRCT pictures. Although this method offers the benefit of removing the reliance on human skill, it will not be able to identify the precise area that is contaminated by ILD and will instead be needed for manual ROI of ILD extraction. The ROI technique will take a long time to scan multiple HRCT pictures. The suggested method, however, will track the entire image in order to assign it to a certain ILD class. The assumption used in developing the proposed ILD classifier is that there is only one type of ILD present in the input HRCT image. To handle input photos containing many ILDs, however, the ILD classifier needs to be enhanced. This should enable it to identify all classes or severe classes in the provided image. Another drawback of the suggested approach is that it can only be used to classify seven important ILDs and is ineffective for many other ILDs such as thickened septa, reticulation, reduced attenuation areas,

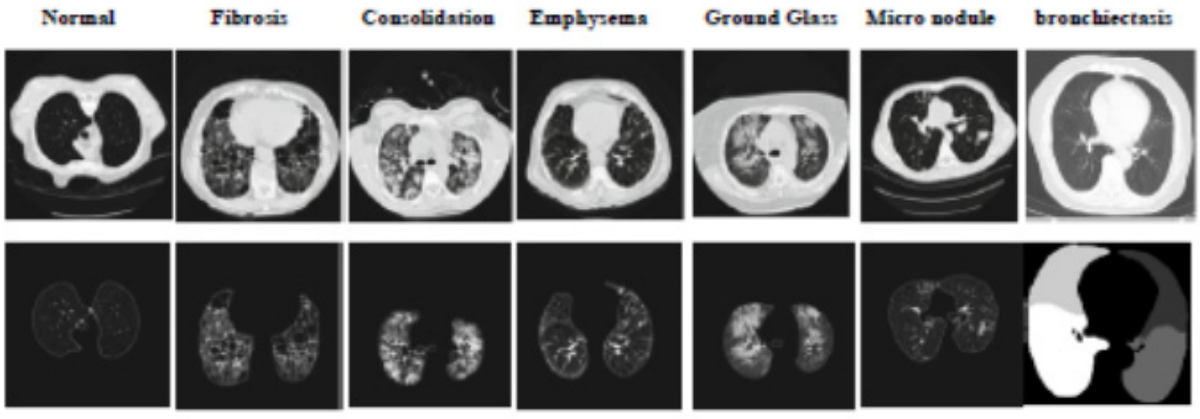

Figure 4: HRCT samples of seven ILDs. (1st row displays the novel HRCT images, while 2nd row displays segmented version of those images).

Table 3: ILD Classifier collaborative performance of the projected algorithm.

	Fibrosis	Emphysema	Ground Glass	Micro-nodules	Normal	Consolidation	Bronchi-tasis	Average
Precision (%)	80.89	98.94	83.57	92.84	91.68	89.96	92.85	89.65
Recall (%)	89.26	93.24	84.44	90.64	94.65	84.12	91.65	89.39
F-score (%)	84.87	96.00	84.00	91.73	93.14	86.94	91.77	89.45
Accuracy	0.9769	0.9960	0.9811	0.9948	0.9969	0.9793	0.9950	0.9875

Table 4: Comparison of the projected classifier with the previous CNN-based classifiers.

Method	F-score (%)	Accuracy (%)
Li *et al.*[17]	66.57	67.05
LeNet.[24]	67.83	67.90
AlexNet.[17]	70.31	71.04
VGGNet.[10]	78.04	78.00
Proposed Classifier	89.55	98.75

honeycombing, lymph nodes and pleura involvement that were not taken into account in this study. Also, one more limitation of suggested approach is that it will not considers PET-CT images, it works only on HRCT images. The use of cutting-edge computational methods in ILD classification has significant effects on pharmaceutical research and teaching. The capacity of the model to yield precise and repeatable outcomes speeds up the diagnostic procedure and promotes a better comprehension of the pathophysiology of ILD. This information is crucial for the creation of targeted treatments since it enables pharmaceutical researchers to create treatments that are customized for particular ILD subtypes.

CONCLUSION

It has been suggested to use whole HRCT images in a two-stage hybrid deep learning network screening method for Interstitial Lung Disease (ILD). The performance of the classifier as a whole has improved as deep learning algorithms' accuracy has increased at each level. First, the background is removed from HRCT images using lung segmentation, allowing the subsequent phase to reliably abstract ILD features from the lung image. Using ResNet50, deep features were extracted from the segmented lung images. To categorize data into seven ILD classes-ground glass, normal, fibrosis, emphysema, micro nodules, consolidation and bronchiectasis-the multiclass support vector machine technique makes use of deep learning features.

The suggested algorithm's performance has compared with that of previous patch-based and whole-image-based techniques. The healthy class has the maximum classification accuracy, at 94.65%, which helps to lessen the likelihood of false alarm situations. The consolidation class has the lowest classification accuracy, which is still extreme higher than other whole-image-based techniques at 84.12%. The suggested technique performs significantly better than previous algorithms that just take into account five ILD classes and outperforms a comparable entire image-based algorithm. The suggested method highlights the possibility for increasing total performance by selecting the best CNN for a particular task and increasing accuracy at each level of the processes. Moreover, the suggested multistage CNN requires very little extra time. The Two-Level Deep Learning Approach that is being introduced here presents a viable way to improve ILD categorization and add to the larger field of pharmaceutical research and teaching.

ACKNOWLEDGEMENT

The authors are very grateful to SKN College of Engg., Pune for providing all facilities to carry out this research.

ETHICS APPROVAL AND CONSENT TO PARTICIPATE

Since the data is taken from http://www.image-net.org, which is available freely, hence no approval is required.

CONFLICT OF INTEREST

The authors declare that there is no conflict of interest.

ABBREVIATIONS

ILD: Interstitial Lung Disease; **HRCT:** High-Resolution Computed Tomography; **CNN:** Convolutional Neural Network; **c-GAN:** Conditional Generative Adversarial Network; **SVM:** Support Vector Machine.

SUMMARY

The suggested approach makes use of entire HRCT images to do away with the need for physical ROI extraction of ILD-infested lung tissue. In the suggested method, the first step involved precise lung segmentation utilizing a conditional generative adversarial network (c-GAN) with a multiscale feature extraction module. In second step, the segmented lung pictures were used to abstract the deep features using ResNet50 and lastly, the Support Vector Machine (SVM) classified the 10 ILD classes using deep features from ResNet50.

REFERENCES

1. H. Yang and E. K. Lee, Healthcare Analytics: From Data to Knowledge to Healthcare Improvement, John Wiley and Sons, 2016.
2. U. Bagci, J. Yao, A. Wu, *et al.*, "Automatic detection and quantification of tree-in-bud (TIB) opacities from CT scans," IEEE Transactions on Biomedical Engineering, 2012;59:1620-32.
3. A. Depeursinge, D. van de Ville, A. Platon, A. Geissbuhler, P. A. Poletti and H. Muller, "Near-affine-invariant texture learning for lung tissue analysis using isotropic wavelet frames," IEEE Transactions on Information Technology in Biomedicine, 2012;16(4):665-75.
4. C. Sluimer, P. F. van Waes, M. A. Viergever and B. van Ginneken, "Computer aided diagnosis in high resolution CT of the lungs," Medical Physics, 2003;30(12):3081-90.
5. M. H. Yap, G. Pons, J. Marti, *et al.*, "Automated breast ultrasound lesions detection using convolutional neural networks," IEEE Journal of Biomedical and Health Informatics, 2018;22(4):1218-26.
6. G. Chen, J. Zhang, D. Zhuo, Y. Pan and C. Pang, "Identification of pulmonary nodules via CT images with hierarchical fully convolutional networks," Medical and Biological Engineering and Computing, 2019;57:1567-80.
7. S. Pang, A. Du, M. A. Orgun and Z. Yu, "A novel fused convolutional neural network for biomedical image classification," Medical and Biological Engineering and Computing, 2019;57:107-21.
8. A. Krizhevsky, I. Sutskever and G. E. Hinton, "Image Net classification with deepconvolutional neural networks," Communications of the ACM, 2017;60:84-90.
9. K. Simonyan and A. Zisserman, "Very deep convolutional networks for large-scale image recognition," 2014, https://arxiv .org/abs/1409.1556.
10. C. Szegedy, W. Liu, Y. Jia, *et al.*, "Going deeper with convolutions," in Proceedings of the IEEE Conference on Computer Vision and Pattern Recognition (CVPR), pp. 1-9, Boston,USA, 2015.
11. S. J. Pan and Q. Yang, "A survey on transfer learning," IEEE Transactions on Knowledge and Data Engineering, 2010;22:1345-59.
12. L. Sorensen, S. B. Shaker and M. de Bruijne, "Quantitative analysis of pulmonary emphysema using local binary patterns," IEEE Transactions on Medical Imaging, 2010;29:559-69.
13. Ye Xu, M. Sonka, G. McLennan, Junfeng Guo and E. A. Hoffman, "MDCT-based 3-D texture classification of emphysema and early smoking related lung pathologies," IEEETransactions on Medical Imaging, 2006;25(4):464-75.
14. Yang Song, Weidong Cai, Yun Zhou and D. D. Feng, "Feature- based image patch approximation for lung tissue classification," IEEE Transactions on Medical Imaging, 2013;32(4):797-808.
15. Y. Uchiyama, S. Katsuragawa, H. Abe, *et al.*, "Quantitative computerized analysis of diffuse lung disease in highresolution computed tomography," Medical Physics, 2003;30(9):2440-54.
16. K. C. Santosh, S. Antani, D. S. Guru and N. Dey, Medical Imaging: Artificial Intelligence, Image Recognition and Machine Learning Techniques, CRC Press, New York, 2020.
17. Q. Li, W. Cai, X. Wang, Y. Zhou, D. D. Feng and M. Chen, "Medical image classification with the convolutional neural network," in 2014 13th International Conference on Control Automation Robotics and Vision (ICARCV), pp. 844-8, Singapore, 2014.
18. M. Anthimopoulos, S. Christodoulidis, L. Ebner, A. Christe and S. Mougiakakou, "Lung pattern classification for interstitial lung diseases using a deep convolutional neural network," IEEE Transactions on Medical Imaging, 2016;(35):1207-16.
19. V. N. Sukanya Doddavarapu, G. B. Kande and B. Prabhakara Rao, "Differential diagnosis of Interstitial Lung Diseases using deep learning networks," The Imaging Science Journal, 2020;68(3):170-8.
20. W. Guo, Z. Xu and H. Zhang, "Interstitial lung disease classification using improved Dense Net," Multimedia Tools and Applications, 2019;(78):30615-26.
21. D. Poap, M. Wozniak, R. Damaševičius and W. Wei, "Chest radiographs segmentation by the use of nature-inspired algorithm for lung disease detection," in 2018 IEEE Symposium Series on Computational Intelligence (SSCI), pp. 2298-2303, Bangalore, India, 2018.
22. A. T. Sahlol, M. Abd Elaziz, A. Tariq Jamal, R. Damaševičius and O. Farouk Hassan, "A novel method for detection of tuberculosis in chest radiographs using artificial ecosystem-based optimization of deep neural network features," Symmetry, 2020;12(7):1146.
23. M. A. Khan, V. Rajinikanth, S. C. Satapathy, *et al.*, "VGG19 network assisted joint segmentation and classification of lung nodules in CT images," Diagnostics, 2021;11(12):2208.
24. P. Isola, J.-Y. Zhu, T. Zhou and A. A. Efros, "Image-to-image translation with conditional adversarial networks," in Proceedings of the IEEE Conference on Computer Vision and Pattern Recognition (CVPR), pp. 5967-5976, Honolulu, USA, 2017.
25. D. Ulyanov, A. Vedaldi and V. Lempitsky, "Instance normalization: the missing ingredient for fast stylization," 2016, https://arxiv.org/abs/1607.08022.
26. K. He, X. Zhang, S. Ren and J. Sun, "Deep residual learning for image recognition," in Proceedings of the IEEE Conference on Computer Vision and Pattern Recognition (CVPR), pp. 770-8, Las Vegas, USA, 2016.
27. A. Depeursinge, A. Vargas, A. Platon, A. Geissbuhler, P. A. Poletti and H. Müller, "Building a reference multimedia database for interstitial lung diseases," Computerized Medical Imaging and Graphics, 2012;36:227-38.
28. E. Hosseini-Asl, J. M. Zurada, G. Gimelfarb and A. El-Baz, "3- D lung segmentation by incremental constrained nonnegative matrix factorization," IEEE Transactions on Biomedical Engineering, 2015;63:952-63.
29. O. Ronneberger, P. Fischer and T. Brox, "U-net: convolutional networks for biomedical image segmentation," in Medical Image Computing and Computer-Assisted Intervention-MICCAI 2015, N. Navab, J. Hornegger, W. Wells and A. Frangi, Eds., vol. 9351 of Lecture Notes in Computer Science, pp. 234-41, Springer, Cham, 2015.
30. Mulani, A. O., Jadhav, M. M., and Seth, M. (2022). Painless Non-invasive blood glucose concentration level estimation using PCA and machine learning. the CRC Book entitled Artificial Intelligence, Internet of Things (IoT) and Smart Materials for Energy Applications.
31. Mulani, A. O., Birajadar, G., Ivković, N., Salah, B., and Darlis, A. R. Deep Learning Based Detection of Dermatological Diseases Using Convolutional Neural Networks and Decision Trees. Traitement du Signal, 2023;40(6).
32. Jadhav, H. M., Mulani, A., and Jadhav, M. M. Design and Development of Chatbot Based on Reinforcement Learning. Machine Learning Algorithms for Signal and Image Processing, 2022;219-29.
33. Kashid, M. M., Karande, K. J., and Mulani, A. O. (2022, November). IoT-Based Environmental Parameter Monitoring Using Machine Learning Approach. In Proceedings of the International Conference on Cognitive and Intelligent Computing: ICCIC 2021, 2022;1:43-51. Singapore: Springer Nature Singapore.
34. Mulani, A. O., Birajadar, G., Ivković, N., Salah, B., and Darlis, A. R. Deep Learning Based Detection of Dermatological Diseases Using Convolutional Neural Networks and Decision Trees. Traitement du Signal, 2023;40(6).

Cite this article: Jadhav VD, Patil LV. Interstitial Lung Diseases Classification in the Context of Pharmaceutical Education and Research: A Two-Level Deep Learning Approach. Indian J of Pharmaceutical Education and Research. 2024;58(3s):s787-s795.